https://doi.org/10.1007/s11434-016-1178-8

A micro photocatalytic fuel cell with an air-breathing, membraneless and monolithic design

Ming Xia[a,b], Rong Chen[a,b]*, Xun Zhu[a,b]*, Qiang Liao[a,b], Liang An[c]*, Zhibin Wang[a,b], Xuefeng He[a,b], Long Jiao[a,b]

[a] Key Laboratory of Low-grade Energy Utilization Technologies and Systems (Chongqing University), Ministry of Education, Chongqing 400030, China

[b] Institute of Engineering Thermophysics, Chongqing University, Chongqing 400030, China

[c] Department of Mechanical Engineering, The Hong Kong Polytechnic University, Hong Kong, China

*Corresponding author:

[a,b] Tel.: 0086-23-65103119; fax: 0086-23-65102474; e-mail: rchen@cqu.edu.cn (Rong Chen)

[a,b] Tel.: 0086-23-65102474; fax: 0086-23-65102474; e-mail: zhuxun@cqu.edu.cn (Xun Zhu)

[c] Tel.: 852-27667820; fax: 852-23654703; e-mail: liang.an@polyu.edu.hk (Liang An)

Abstract

In this study, a membraneless, monolithic micro photocatalytic fuel cell with an air-breathing cathode was developed for simultaneous wastewater treatment and electricity generation. In this newly-developed micro photocatalytic fuel cell, the photoanode and cathode were arranged with a shoulder-to-shoulder design, forming two planar electrodes. Such design offers several advantages of enhanced mass transfer, uniform light distribution, short light transfer path, membrane elimination and easy fabrication, integration, and compatibility with other microdevices. The performance of this type fuel cell was evaluated by using methanol as a model pollutant under the alkaline condition. Experimental results indicated the developed micro photocatalytic fuel cell was able to show good photo-response to the illumination and satisfactory performance as well as durability. Parametric study on

the cell performance was also performed. It was found that increasing the light intensity, methanol concentration and KOH concentration could improve the cell performance. But for the effect of the liquid flow rate, it was shown that the cell performance firstly increased with increasing the liquid flow rate and then decreased with further increasing the liquid flow rate. This study not only opens a new avenue for the design of the micro photocatalytic fuel cell but also is helpful for the optimization of the operating conditions.

Keywords: Photocatalytic fuel cell; Membraneless and monolithic design; Air-breathing cathode; Photo-response; Cell performance

1. Introduction

With the economic development, people become more concerned about the environmental problems all over the world. In particular, every year a huge amount of wastewater is discharged to natural ecosystem, which greatly threatens aquatic life and human health [1-3]. Hence, the wastewater treatment has become an issue of global concern, especially in developing countries [4]. To resolve this issue, several approaches have been developed, including the biodegradation [5-7], adsorption [8, 9], chemical oxidation [10] and so on [11, 12]. On the other hand, it should be recognized that although the discharge of wastewater causes a severe environmental problem [13], wastewater contains numerous organics [12, 14], which is an available energy source. However, the above-mentioned conventional wastewater treatment technologies usually aim at the efficient degradation of these organics. The chemical energy stored in wastewater is not efficiently utilized, leading to the energy loss. Therefore, recovering the energy released from organic pollutants in wastewater during the treatment is promising to address the environmental and energy problems simultaneously [15, 16], but still challenging.

Photocatalytic fuel cell (PFC), which is an integration of the photocatalysis and fuel cell technologies, is one of ideal solutions to simultaneously address the wastewater and energy recovery issues. Unlike conventional fuel cells, in which noble metals are usually employed to oxidize the simple organic compounds, the PFCs use the abundant materials of semiconductors [17] as the catalysts to form the photoanode,

which greatly lowers the capital cost. Upon illumination, the absorbed photons ensure the electron-hole pairs to be generated in the semiconductors. The photo-generated holes can firstly oxidize OH^- to hydroxyl radicals (·OH), which are powerful oxidants [18, 19] and then degrade the organic compounds into CO_2 and H_2O. The photo-generated electrons spontaneously flow to the cathode through an external circuit to form the electricity. As a result, the PFCs enable simultaneous wastewater treatment and electricity production [20-24]. Moreover, PFCs can degrade most organic compounds such that the fuel type limitation in conventional fuel cells can be avoided [8]. Because of these advantages, the PFC has received ever-increasing attention.

Since the performance of the PFC mainly depends on the photocatalysts, extensive efforts have been devoted to the development of materials over the past decade [25-29]. These works mainly aimed to promote the photoelectrochemical oxidation rate and reduce charge transport resistance. Besides, the photon and mass transport also play important roles in the PFC performance, which is inherently associated with the cell design. However, the design of the PFC has not been widely explored. Most existing PFCs have large dimensions. Such design usually has the problem of low specific surface area and mass transfer rate. The ion exchange membrane is also typically required to separate the PFC into two compartments of the anode and cathode, respectively [22, 30]. The use of the ion exchange membrane definitely increase the capital cost of the PFC. Moreover, conventional PFCs usually adopt the

mode of the oxygen-dissolved electrolyte at the cathode. Because of the low solubility of oxygen, the cathode performance of the PFC is restricted. All these disadvantages arising from the conventional PFC design with large scale dimension limit its performance improvement.

Recently, the incorporation of microfluidics into the photocatalytic technologies opens a new avenue for enhancing the performance of the PFC. Owing to its intrinsic merits of large surface-to-area ratio, fine flow control and enhanced heat and mass transfer, the microfluidic platform has been successfully applied to water splitting [31], wastewater treatment [32] and so on [33, 34]. In particular, the microfluidics enables uniform light distribution and short light transfer path. Under such circumstance, along with enhanced mass transfer by the microfluidic platform, the photocatalytic reaction rate can be greatly improved. Inspired by this idea, a membraneless monolithic micro PFC (μPFC) with an air-breathing cathode was developed in this study. Unlike the previously-reported membraneless micro PFC with an air-breathing cathode [32], in which the photoanode and cathode were face-to-face, the photoanode and cathode were arranged with a shoulder-to-shoulder design in this study, forming two planar electrodes. In addition to the above-mentioned advantages, this new design also offers the following advantages. First, the membrane elimination not only reduces the capital cost but also makes the membrane-related issues such as membrane fouling disappear. Second, the air-breathing design can greatly enhance the oxygen transport as compared to the oxygen-dissolved mode and simplify the cell

system. Third, this simple design benefits for the fabrication (e.g., replication), integration, and compatibility with other microdevices [35, 36]. To demonstrate the feasibility of this new design of μPFC, methanol was used as a model fuel to examine the performance of the developed μPFC in an alkaline environment under the UV illumination. The photo-response and its durability were studied, as well as the effects of the methanol concentration, KOH concentration, light intensity and liquid flow rate.

2. Materials and methods

2.1 Design of μPFC and working principle

As sketched in Fig. 1, the μPFC developed in this work mainly consisted of a cover, a photoanode, a cathode and a baseplate. The cover was made of Polydimethylsiloxane (PDMS). In this cover, there were two microchambers for the photoanode and cathode, respectively. Each microchamber had one inlet and one outlet. A FTO glass with the dimension of 30 mm × 50 mm (resistance 10 Ω per square, Xinyan Technology Co., China) was chosen to fabricate the photoanode. In the middle, the conducting layer with a width of 1.0 mm was removed by the etching method to separate the photoanode and cathode and avoid the short circuit. On one side of this line, the photoanode was fabricated by coating TiO_2 on the FTO glass with the dimension of 24 mm × 4.5 mm. A rectangular shape hole with the dimension of 10 mm × 24 mm was drilled on the other side of this line for positioning the cathode and breathing oxygen from air. A commercial cathode of the Pt coated carbon paper (DMFC

Cathode, Alfa Aesar, Great Britain) was chosen as the air-breathing cathode, which was tailored into T shape. As shown in Fig. 1a (right portion), the straight part was the active area for oxygen reduction reaction with a dimension of 24 mm × 4.5 mm and the remaining part was functioned as current collection. The baseplate was also made of PDMS with the same dimension as the FTO glass. There was a convex plate on the baseplate, which faced the drilled hole in the FTO glass. Meanwhile, there was also a drilled hole with a dimension of 20 mm × 3 mm. The function of this convex plate was to support the cathode and simultaneously ensure the surface of the cathode to be at the same horizon with the photoanode, while the oxygen from air was transferred via the drilled hole.

The working principle of the developed μPFC is illustrated in Fig. 1b. During the operation, the methanol solution along with KOH is supplied to the photoanode microchamber and the KOH solution is supplied to the cathode, while oxygen is from the ambient air. Once the UV-light illuminates the photoanode, the electrons (e^-) in the valence band of photocatalyst are excited to the conduction band, and the holes (h^+) are simultaneously generated. The holes react with OH^- to produce hydroxyl radicals that are strong oxidant. Methanol can then be oxidized to CO_2 and H_2O by the photoelectrochemical reactions, as represented by reactions (1) and (2).

$$h\nu + TiO_2 \rightarrow TiO_2 + e^- + h^+ \quad (1)$$

$$6h^+ + CH_3OH + 6OH^- \rightarrow CO_2 + 5H_2O \quad (2)$$

$$2H_2O + O_2 + 4e^- \rightarrow 4OH^- \quad (3)$$

The generated electrons then go through the external load to the cathode. At the cathode, electrons react with oxygen and water to produce OH^-, which can be described by the reaction (3). The produced OH^- ions directly cross to the photoanode to complete the photoanode reactions.

2.2 Preparation of the photoanode

The preparation of the photoanode on the FTO glass is illustrated in Fig. 2. First of all, a 30 mm×50 mm FTO glass was cut. Close to the middle line with a width of 1 mm, a 10 mm × 24 mm hole was drilled by laser drilling for positioning the cathode and breathing oxygen from air. Second, the dilute hydrochloric acid along with zinc powder was used to remove the conducting layer on the middle line by the chemical etching such that the electrical isolation between the photoande and cathode could be ensured. Third, the TiO_2 nanoparticles were coated on the photoanode. To do this, the TiO_2 colloid was firstly prepared using a spray painting method. Here, 12 g TiO_2 nanoparticles (Aeroxide P25, Acros, Belgium), 120 mL DI water and 0.4 mL acetylacetone (Sigma-Aldrich, USA) were mixed with magnetic stirring. 0.2 mL of a Triton X-100 (Sigma-Aldrich, USA) and 2.4 g polyethylene glycol (Aladdin, China) were put into the mixture and then magnetically stirred for 12 hours. After that, the TiO_2 colloid was sprayed onto the FTO glass by a spray gun followed by the calcinations at 550 °C for 2 h to form a TiO_2 film on the FTO glass as the photoanode. The TiO_2 loading was about 3 mg/cm^2.

2.3 Preparation of the cover and baseplate

The cover and the baseplate were both made of PDMS. Before the preparation, two molds were firstly made by aluminium for the cover and baseplate, respectively. For the cover mold that was male mould, two 24 mm × 4.5 mm microchambers with the distance of 1 mm between them and the depth of 0.9 mm were milled. To supply the liquid solution uniformly, at both the inlets and outlets, a triangular shape channel was designed and connected with the microchambers. Note that at the fabricated male mould, another line-shape concave plate with the depth of 0.5 mm between the photoanode and cathode was milled. For the baseplate, a cavity block type mold was fabricated. Here, a 10 mm × 24 mm cavity with a 3 mm × 20 mm convex plate at desired location was milled. After the fabrication of these two molds, polymer base (Sylgard 184 A, Dow Coming) and curing agent (Sylgard 184 B, Dow Coming) were mixed with a ratio of 10:1 and degassed. This mixture was then poured into the fabricated moulds and baked at 100 ℃ for 20 min. Finally, the PDMS sheets were released from the moulds. As such, the cover with two microchambers of 24 mm × 4.5 mm × 0.9 mm and the baseplate with a 3 mm × 20 mm hole illustrated in Fig. 1a could be achieved. Moreover, because of the existence of the line-shape concave plate at the cover mold, the connection area between the photoanode and cathode in the formed cover could be reduced, which helped to reduce the direct transport of methanol from the photoanode to the cathode.

2.4 Assembly of the μPFC

With the prepared photoanode, cathode, cover and baseplate, the μPFC could be formed by assembling them. First, the photoanode was assembled with the baseplate. During the assembly process, the drilled hole faced the convex plate on the baseplate. The tailored cathode was put on the drilled hole and simultaneously the same horizon between the cathode surface and photoanode was ensured. Four 2.5-mm holes were drilled in the cover, which were then connected with a needle, respectively. Then the cover was placed on the photoanode. After that, to prevent the leakage, the PDMS was used to seal the gaps between these components and then baked again. As such, a membraneless and monolithic μPFC with an air-breathing cathode was formed. The image of the fabricated μPFC is given in Fig. 3.

2.5 Experimental instruments

In this study, a 100 W LED (Lightwells, Shenzhen, China) with the wavelength of 365 nm was used as light source. The UV light intensity was controlled by adjusting the distance between the μPFC and light source, and measured by an IR-radiometer (UV-A, Photoelectric Instrument Factory of Beijing Normal University, China). The methanol-electrolyte mixed solution and electrolyte solution were introduced into the photoanode and cathode of the μPFC by a syringe pump (Pump 33, Harvard, America) and the flow rate was controlled by this pump. During all experiments, the liquid flow rates at both the photoanode and cathode always remained the same to ensure the laminar flow. The KOH concentrations at both the photoanode and cathode also always remained the same. Spectral energy absorption was measured by a UV-vis

spectrophotometer (UV-2100, Shimadzu Corporation, Japan). Electrochemical measurements were carried out with an electronic load system (CT-3008, Neware Technology Ltd., China) and a data collecting instrument (34972A, Angilet, America).

3. Results and discussion

3.1 Characterization of the photoanode

The morphology of the prepared photoanode on the FTO glass was characterized by the scanning electron microscope (SEM, S-4800, Hitachi, Japan). The results are shown in Fig. 4. From the top view of Fig. 4a, it can be seen that the TiO_2 nanoparticles tended to form clusters, which were then uniformly distributed on the FTO glass. Numerous micro pores with the pore size ranging from tens of nanometers to hundreds of nanometers were formed. Such porous structure not only provides large specific surface area for the photoreactions but also offers plenty of pathway for the mass and photon transport. Figure 4b displays the cross-section view of the prepared photoanode. The morphology obtained at the cross section was similar to the one obtained from the top view, further indicating that a uniform porous TiO_2 film with a wide pore size distribution was successfully prepared. Moreover, from the cross-section view, the thickness of this film could also be determined, about 26 μm. In addition to the microscopic morphology, the absorption spectra of the prepared TiO_2 film were also measured. Figure 5 shows the UV-Vis diffusion reflectance spectra from 240 to 800 nm of the prepared TiO_2 film. It is clear that the majority of absorbed light was below 400 nm in the UV-Vis spectra because the pure TiO_2 was

employed to prepare the photoanode in this work.

3.2 Photo-response of the photoanode

As a photocatalytic fuel cell, because the oxidation of the organic compounds occurs at the photoanode, which is initiated by the illumination, the first one to assess the μPFC performance is to study the photo-response of the photoanode. Fig. 6 shows the photo-response behaviors of the μPFC under the light on/off cycles. In this measurement, the light intensity was 6 mW/cm^2, the methanol concentration was 1.0 mol/L and the KOH concentration was 0.5 mol/L. The flow rates at both the photoanode and cathode remained at 200 μL/min. The photo-response behavior of the cell voltage to the illumination is shown in Fig. 6a. Here, the open circuit voltage (OCV) was used to examine the photo-response of the cell voltage. As seen in Fig. 6a, when the UV light was illuminated to the μPFC, the OCV was immediately increased and stabilized at about 1.16 V in a few seconds. When the light was switched off, the OCV was quickly restored to the state without the illumination. In the four testing cycles, the OCV could well repeatedly respond to the illumination. The photo-response of the photocurrent was also characterized in this work. As mentioned earlier, the μPFC was able to remove the organic compounds and simultaneously generate electricity. The maximum degradation efficiency usually responds to the largest photocurrent density, *i.e.*, short circuit current density. Hence, when characterizing the photo-response of the photocurrent, the short circuit current density was chosen as a representative current density. Fig. 6b shows the results on the

photo-response of the short circuit current density to the illumination. As seen in Fig. 6b, once the light was illuminated to the photoanode, the short circuit current density was instantly shifted from 0 to about 0.65 mA/cm^2. When the light was off, the short circuit current density was immediately decreased to zero. Similarly, in the four testing cycles, the short circuit current density could well repeatedly respond to the illumination. In summary, the photo-responses of the OCV and short circuit current density could be well reproduced in these four light on/off cycles. This fact implies that the developed μPFC is able to well respond to the illumination and a good photo-responsive performance has been attained.

3.3 General discharging performance of the μPFC

The polarization curve and long-term discharging performance have been widely used to characterize the cell performance in conventional fuel cells. In this work, therefore, we also employed these two measures to evaluate the performance of the developed μPFC. In this testing, the light intensity, methanol concentration and KOH concentration were 6 mW/cm^2, 1.0 and 0.5 mol/L, respectively. The flow rates at the photoanode and cathode both remained at 200 μL/min. The typical polarization curve under given condition is presented in Fig. 7a, which shows the cell voltage reduced with the current density increasing. At low current densities (<0.05 mA/cm^2), the cell performance was mainly dependent on the kinetics at both the photoanode and cathode. Therefore, the cell voltage showed a relatively quick reduction in the cell voltage. As the current density increased, the ohmic loss became dominant in the cell

discharging behavior. As a result, the cell voltage linearly declined with increasing the current density. However, when the current density exceeded 0.5 mA/cm^2, the cell voltage reduced sharply. A peak power density of 0.4 mW/cm^2 was obtained at the current density of 0.5 mA/cm^2 under this typical condition. Such dramatic reduction in the cell voltage may be caused by two reasons. One is that at high current densities, the demand of the supplied fuel was increased. For a given methanol concentration and flow rate, the polarization associated with the mass transfer became more serious at high current densities, resulting in a relatively quick reduction in the cell voltage. On the other hand, at high current densities, the cell voltage was small. The driving force for transferring excited electrons to the cathode was weakened. Accordingly, the electrons and holes were easily recombined at the photoanode, which in turn made the cell voltage dramatically drop. It should be pointed out that although the mass transfer issue contributes to the decrease of the cell voltage at high current densities, the re-combination of the electron-hole pairs might be dominant because the limiting current density was not high as compared to the supplied methanol concentration and liquid flow rate.

In practice, the fuel cell is usually operated at a given cell voltage or current density. In this case, the long-term performance of the developed μPFC needs to be characterized to explore its performance and stability. To do this, the long-term performance of the developed μPFC was measured at a constant current density of 0.35 mA/cm^2 for 3 hours. Similarly, the methanol and KOH concentrations were

maintained at 1.0 and 0.5 mol/L, while the light intensity and flow rates at both electrodes were kept at 6 mW/cm^2 and 200 μL/min, respectively. As shown in Fig.7b, the cell voltage of the μPFC was very stable. During the 3 h continuous operation, the cell voltage just slightly decreased from 0.94 to 0.89 V, only accounting for 5.3 % reduction. This result indicates that the membraneless and monolithic design enables the flow state to be well maintained at the laminar flow and the sufficient oxygen can be stably supplied, both of which ensure a rather stable long-term performance of the developed μPFC for future applications.

3.4 Effect of the light intensity

As one of the new energy technologies, the photoelectrochemical reactions at the photoanode of the μPFC are actuated by the incident light. No doubt, the light intensity has an important influence on the performance of the μPFC. For this reason, the effect of the light intensity on the μPFC performance was studied in this work. In the testing, the methanol concentration was 1.0 mol/L, the KOH concentration was 0.5 mol/L and the flow rates at both the photoanode and cathode were 200 μL/min. The light intensity ranged from 2 to 8 mW/cm^2. The polarization and power density curves of the μPFC under different light intensities are shown in Fig. 8a and 8b, respectively. As shown in Fig. 8a, as the light intensity increased, the OCV of the μPFC was improved. Clearly, the stronger the light intensity, the more photo-generated electron–hole pairs. Under such a circumstance, more hydroxyl radicals that are strong oxidant could be generated to promote the

photoelectrochemical reactions at the photoanode. That is why the OCV increased with increasing the light intensity. Due to the same reason, more photo-excited electrons could allow for an increase in the limiting current density. On the other hand, because more hydroxyl radicals could be generated at high light intensity, the enhanced photoelectrochemical kinetics slowed down the decreasing rate of the cell voltage, as evidenced by the decrease of the slope shown in Fig. 8a. Because of these reasons, the limiting current density increased from 0.21 to 0.63 mA/cm^2 with increasing the light intensity from 2 to 8 mW/cm^2. It is interesting to notice that although the limiting current density increased with the light intensity, the supplied methanol concentration and flow rates remained unchanged. In this case, it is clear that the limiting current density caused by the sharp reduction of the cell voltage at high current densities should not be in association with the mass transfer limitation. As mentioned above, the sharp reduction of the cell voltage was caused by easy recombination of the electron-hole pairs at high current densities corresponding to low cell voltage, which can also be proved by the cell voltage turning to be dramatically decreased. As shown in Fig. 8a. The cell voltages under all light intensities started to sharply decrease at the almost same cell voltage of about 700 mV, This fact implied that at this critical cell voltage, the recombination of the electron-hole pair became rather severe, limiting the improvement in the current density. However, high light intensity could enhance the photoelectrochemical kinetics. Along with the increased OCV, the limiting current density increased with the light intensity. Corresponding to the polarization curve, the variation in the power

density with the current density of the μPFC was achieved and the results are shown in Fig. 8b. Increasing the light intensity from 2 to 8 mW/cm^2 resulted in an increase in the peak power density from 0.14 to 0.48 mW/cm^2. In summary, the increase of the light intensity could promote the photoanode reactions because of more photo-excited electron-hole pairs. Hence, the developed μPFC could exhibit a considerable improvement in the cell performance at high light intensity.

3.5 Effect of the methanol concentration

Fig. 9 shows the effect of the methanol concentration on the performance of the μPFC. In this section, the methanol concentration varied from 0.05, 1.0, 2.0 to 4.0 mol/L. The light intensity was 6 mW/cm^2, the KOH concentration was 0.5 mol/L and the liquid flow rates at both the photoanode and cathode were 200 μL/min. It can be seen from Fig. 9 that the performance of the μPFC was affected by the methanol concentration. Increasing the methanol concentration from 0.05 to 4.0 mol/L resulted in an increase in the limiting current density from 0.52 to 0.65 mA/cm^2. In addition to the increase of the limiting current density, the OCV also increased with the methanol concentration. This is due to the enhanced mass transport of methanol. In this case, the efficient hole scavenging by methanol could liberate more free electrons, making the photoanode potential more electronegative and thus increasing the potential difference between the photoanode and cathode [37]. As a result, the OCV increased with increasing the methanol concentration. Besides the hole scavenger contribution, the enhanced methanol transport by increasing the supplied methanol concentration

led to the improvement in the methanol concentration at the liquid/solid interface, which also accelerated the photoelectrochemical reactions. Therefore, the limiting current density improved with the methanol concentration. In addition, it is also interesting to find that, similar to the sharp reduction in the cell voltage at high current densities for the effect of the light intensity, such a sharp reduction was also observed at the cell voltage of about 700 mV due to the electron-hole pair recombination when changing the methanol concentration. Hence, the competition between these effects made the increment relatively small. With the polarization curves, the power density *vs* the current density could also be achieved and the results are shown in Fig. 9b. As seen, when the methanol concentration was increased from 0.05 to 4.0 mol/L, the peak power density increased from 0.37 to 0.48 mW/cm^2. However, it should be noted that too high methanol concentration may cause more methanol to diffuse to the cathode, increasing the mixed potential at the cathode and lowering the cathode performance. Therefore, too high methanol concentration may not be favorable for the cell performance improvement.

3.6 Effect of the KOH concentration

It is well known that the OH^- ions can function as the hole scavengers to prevent the recombination of the photo-generated electron-hole pairs. Hence, the electrolyte concentration, i.e., the KOH concentration has a significant influence on the cell performance. For this reason, the effect of the KOH concentration was explored in this study. To do this, the methanol concentration was set as 1.0 mol/L, the light

intensity was 6 mW/cm^2 and the flow rates at both the photoanode and cathode were 200 μL/min. The KOH concentration ranged from 0.01 to 1.0 mol/L at both the photoanode and cathode.

Fig. 10a shows the polarization curves of the μPFC with different KOH concentrations varying from 0.01 to 1.0 mol/L. It can be seen that increasing the KOH concentration from 0.01 to 1.0 mol/L resulted in an increase in the limiting current density from 0.34 to 0.56 mA/cm^2. Moreover, the OCV was also increased. Three reasons contributed to these phenomena. First, the increased KOH concentration indicated that more OH^- ions were supplied to the μPFC. OH^- ions were able to efficiently scavenge holes to generate more hydroxyl radicals so that the recombination of the electron-hole pair can be efficiently hindered. As a result, the photoeletrochemical reaction kinetics at the photoanode can be greatly improved, leading to the increase of the cell performance. Second, the increased KOH concentration can also facilitate the oxygen reduction reaction at the cathode, which helps to improve the cathode potential and thus the cell performance. Third, as mentioned above, during the working process of the μPFC, the OH^- ions were generated at the cathode and then transported to the photoanode, at which they were consumed. Therefore, the change of the KOH concentration can also affect the transport of the OH^- ion and thereby the ohmic loss of the cell. In particular, at the extremely low KOH concentration (0.01 mol/L), because of poor conductivity of the OH^- ion, the ohmic loss became rather critical. This can be proved by comparing the

slope at moderate current densities. As seen, the slope with the KOH concentration of 0.01 mol/L was much larger than those with high KOH concentrations, indicating that the ohimic loss led to a quick reduction in the cell voltage. Therefore, because of these three reasons, the cell performance improved with increasing the KOH concentration. Corresponding to the polarization curves, the change of the power density with the current density was obtained and the results are shown in Fig. 10b. Increasing the KOH concentration resulted in an increase in the peak power density from 0.16 to 0.41 mW/cm^2. The above results indicate that in the testing range, increasing the KOH concentration facilitates the improvement in the cell performance.

3.7 Effect of the flow rate

In this novel design of the μPFC, two electrodes were arranged in parallel on a chip. The fuel and electrolyte solutions were continuously supplied to the μPFC with the same flow rate, respectively. In this case, the mass transfer at both the photoanode and cathode is influenced by the flow rate. For this reason, the effect of the flow rate on the cell performance was also investigated. In this testing, the methanol concentration was 1.0 mol/L, the KOH concentration was 0.5 mol/L and light intensity was 6 mW/cm^2. The flow rate ranged from 10 to 1200 μL/min. The effect of the flow rate on the performance of the μPFC is shown in Fig. 11.

Fig. 11a shows the variation of the polarization curve of the μPFC with the flow rate.

It can be seen that when the current density was below 0.3 mA/cm^2, the flow rate showed little effect on the cell performance. As the current density increased, the flow rate started to be an influential factor to the cell performance. As shown in Fig. 11a, the cell performance, including the limiting current density, was firstly increased as the flow rate was increased from 10 to 200 μL/min. At critically low flow rate, the residence time was larger, which benefited for the performance improvement. However, if the flow rate was too small, the mass transport of methanol and OH^- ion was poor. Accordingly, the photoelectrochemical and electrochemical reactions at the respective photoanode and cathode became sluggish so that the cell performance became low. As the flow rate was increased to 200 μL/min, this problem was resolved and thus the cell performance was improved. However, as the flow rate was further increased, the residence time became much smaller. Under such a circumstance, the limited residence time could not guarantee the efficient photoelectrochemical oxidation of methanol, causing the cell performance to be degraded. For this reason, a maximum peak power density was yielded at the flow rate of 200 μL/min, as shown in Fig. 11b. From these results, it can be found that there existed a liquid flow rate leading to the maximum cell performance, including the limiting current density and peak power density.

To further demonstrate the feasibility of μPFC, we also compared our experimental data with Refs. [38-42]. As shown in Table 1, the peak power density achieved in this work was larger than those of most PFCs. Although there was some work that showed

better performance than ours, they used TiO_2 nano-rod array as the photocatalyst [42], which was able to offer higher light-harvesting efficiency and less charge transfer resistance than TiO_2 nanoparticles. In summary, the developed membraneless monolithic μPFC with the air-breathing cathode is potentially feasible for the future applications.

4. Conclusions

In this study, a membraneless, monolithic micro photocatalytic fuel cell with an air-breathing cathode was developed for simultaneous wastewater treatment and electricity generation. This new design offers several advantages of large specific surface area, enhanced mass transfer, uniform light distribution, short photon transfer path, easy fabrication and integration, and compatibility with other microdevices. The performance of the newly-developed μPFC was evaluated by using methanol as a model pollutant. Experimental results indicated the developed μPFC yielded good photo-response to the illumination and satisfactory performance and durability. Besides, the effects of the light intensity, methanol concentration, KOH concentration and liquid flow rate on the cell performance were also investigated. Parametric studies indicated that increasing the methanol concentration could improve the cell performance as a result of enhanced mass transport to liberate more free electrons and facilitate the photoelectrochemical reactions at the photoanode. An increase in the light intensity led to the improved cell performance because of more generated electron-hole pairs. The increase of the KOH concentration could enhance the

photoelectrochemical and electrochemical reactions at the photoanode and cathode, respectively, and the OH^- ion transport between these two planar electrodes, thereby improving the cell performance. There existed an optimal flow rate to yield the best performance of the μPFC. The obtained results in this study are helpful for the design and operation of such a micro photocatalytic fuel cell in the future.

Acknowledgments

The authors gratefully acknowledge the financial supports of the National Natural Science Foundation of China (51576021, 51222603, 51276208 and 51325602) and the National High-Tech R&D Program of China (2015AA043503).

Conflict of interest

The authors declare that they have no conflict of interest.

References

[1] Smol JP (2009) Pollution of lakes and rivers: a paleoenvironmental perspective. John Wiley & Sons

[2] Deblonde T, Cossu-Leguille C, Hartemann P (2011) Emerging pollutants in wastewater: a review of the literature. Int J Hyg Environ Health 214:442-448

[3] Malmqvist B, Rundle S (2002) Threats to the running water ecosystems of the world. Environ Conserv 29:134-153

[4] Vörösmarty CJ, McIntyre PB, Gessner MO et al (2010) Global threats to human water security and river biodiversity. Nature 467:555-561

[5] Orhon D, Okutman D, Insel G (2002) Characterisation and biodegradation of settleable organic matter for domestic wastewater. Water SA 28:299-306

[6] Joss A, Zabczynski S, Göbel A et al (2006) Biological degradation of pharmaceuticals in municipal wastewater treatment: proposing a classification scheme. Water Res 40:1686-1696

[7] Qualls RG, Haines BL (1992) Biodegradability of dissolved organic matter in forest throughfall, soil solution, and stream water. Soil Sci Soc Amer J 56:578-586

[8] Azhar MR, Abid HR, Sun H et al (2016) Excellent performance of copper based metal organic framework in adsorptive removal of toxic sulfonamide antibiotics from wastewater. J Colloid Interface Sci 478:344-352

[9] Davis J A, Gloor R (1981) Adsorption of dissolved organics in lake water by aluminum oxide. Effect of molecular weight. Environ Sci Technol 15:1223-1229

[10] Pena M, Coca M, Gonzalez G et al (2003) Chemical oxidation of wastewater from molasses fermentation with ozone. Chemosphere 51:893-900

[11] Oh JY, Choi SD, Kwon HO et al (2016) Leaching of polycyclic aromatic hydrocarbons (PAHs) from industrial wastewater sludge by ultrasonic treatment. Ultrason Sonochemistry 33:61-66

[12] Lefebvre O, Moletta R (2006) Treatment of organic pollution in industrial saline wastewater: a literature review. Water Res 40:3671-3682

[13] Eckenfelder WW, Englande AJ (1996) Chemical/petrochemical wastewater management—past, present and future. Water Sci Technol 34:1-7

[14] Reemtsma T, Jekel M (1997) Dissolved organics in tannery wastewaters and their

alteration by a combined anaerobic and aerobic treatment. Water Res 31:1035-1046

[15] Andreozzi R, Caprio V, Insola A et al (1999) Advanced oxidation processes (AOP) for water purification and recovery. Catal Today 53:51-59

[16] Pant D, Singh A, Van Bogaert G et al (2012) Bioelectrochemical systems (BES) for sustainable energy production and product recovery from organic wastes and industrial wastewaters. RSC Adv 2:1248-1263

[17] Li J, Wu N (2015) Semiconductor-based photocatalysts and photoelectrochemical cells for solar fuel generation: a review. Catal Sci Technol 5:1360-1384

[18] Pelentridou K, Stathatos E, Karasali H et al (2009) Photodegradation of the herbicide azimsulfuron using nanocrystalline titania films as photocatalyst and low intensity black light radiation or simulated solar radiation as excitation source. J Hazard Mater 163:756-760

[19] Lianos P (2011) Production of electricity and hydrogen by photocatalytic degradation of organic wastes in a photoelectrochemical cell: the concept of the Photofuelcell: a review of a re-emerging research field. J Hazard Mater 185:575-590

[20] Kaneko M, Ueno H, Ohnuki K et al (2007) Direct electrical power generation from urine, wastes and biomass with simultaneous photodecomposition and cleaning. Biosens Bioelectron 23:140-143

[21] Canterino M, Di Somma I, Marotta R et al (2009) Energy recovery in wastewater decontamination: simultaneous photocatalytic oxidation of an organic substrate and electricity generation. Water Res 43:2710-2716

[22] Antoniadou M, Lianos P (2009) Near ultraviolet and visible light photoelectrochemical degradation of organic substances producing electricity and hydrogen. J Photoch Photobio A 204:69-74

[23] Kaneko M, Ueno H, Saito R et al (2009) Biophotochemical cell (BPCC) to photodecompose biomass and bio-related compounds by UV irradiation with simultaneous electrical power generation. J Photoch Photobio A 205:168-172

[24] Kaneko M, Suzuki S, Ueno H et al (2010) Photoelectrochemical decomposition of bio-related compounds at a nanoporous semiconductor film photoanode and their photocurrent–photovoltage characteristics. Electrochim Acta 55:3068-3074

[25] Díaz-Real JA, Ortiz-Ortega E, Gurrola MP et al (2016) Light-harvesting Ni/TiO_2 nanotubes as photo-electrocatalyst for alcohol oxidation in alkaline media. Electrochim Acta 206:388-399

[26] Beranek R, Neumann B, Sakthivel S et al (2007) Exploring the electronic structure of nitrogen-modified TiO_2 photocatalysts through photocurrent and surface photovoltage studies. Chem Phys 339:11-19

[27] Zhai C, Zhu M, Pang F et al (2016) High efficiency photoelectrocatalytic methanol oxidation on CdS quantum dots sensitized Pt electrode. ACS Appl Mater Inter 8:5972-5980

[28] Thomalla M, Tributsch H (2006) Photosensitization of nanostructured TiO_2 with WS_2 quantum sheets. J Phys Chem B 110:12167-12171

[29] Ma H, Wang H, Wu T et al (2016) Highly active layered double hydroxide-derived cobalt nano-catalysts for p-nitrophenol reduction. Appl Catal B

Environ 180:471-479

[30] Antoniadou M, Vaiano V, Sannino D et al (2013) Photocatalytic oxidation of ethanol using undoped and Ru-doped titania: acetaldehyde, hydrogen or electricity generation. Chem Eng J 224:144-148

[31] Li L, Chen R, Liao Q et al (2014) High surface area optofluidic microreactor for redox mediated photocatalytic water splitting. Int J Hydrogen Energ 39: 19270-19276

[32] Li L, Wang G, Chen R et al (2014) Optofluidics based micro-photocatalytic fuel cell for efficient wastewater treatment and electricity generation. Lab Chip 14:3368-3375

[33] Zhou Y, Basu S, Wohlfahrt KJ et al (2016) A microfluidic platform for trapping, releasing and super-resolution imaging of single cells. Sensor Actuat B Chem 232:680-691

[34] Wang Y, Xu H, Luo J et al (2016) A novel label-free microfluidic paper-based immunosensor for highly sensitive electrochemical detection of carcinoembryonic antigen. Biosens Bioelectron 83:319-326

[35] Tominaka S, Ohta S, Osaka T et al (2011) Prospects of on-chip fuelcell performance: improvement based on numerical simulation. Energ Environ Sci 4:162-171

[36] Tominaka S, Ohta S, Obata H et al (2008) On-chip fuel cell: micro direct methanol fuel cell of an air-breathing, membraneless, and monolithic design. J Am Chem Soc 130:10456-10457

[37] Antoniadou M, Sfaelou S, Lianos P (2014) Quantum dot sensitized titania for

photo-fuel-cell and for water splitting operation in the presence of sacrificial agents. Chem Eng J 254:245-251

[38] Kaneko M, Nemoto J, Ueno H et al (2006) Photoelectrochemical reaction of biomass and bio-related compounds with nanoporous TiO_2 film photoanode and O_2-reducing cathode. Electrochem Commun 8:336-340

[39] Shu D, Wu J, Gong Y et al (2014) BiOI-based photoactivated fuel cell using refractory organic compounds as substrates to generate electricity. Catal Today 224:13-20

[40] Ueno H, Nemoto J, Ohnuki K et al (2009) Photoelectrochemical reaction of biomass-related compounds in a biophotochemical cell comprising a nanoporous TiO_2 film photoanode and an O_2-reducing cathode. J Appl Electrochem 39:1897-1905

[41] Antoniadou M, Kondarides DI, Labou D et al (2010) An efficient photoelectrochemical cell functioning in the presence of organic wastes. Solar Energ Mater Solar Cells 94:592-597

[42] Zhang H, Wang H, Leung MKH et al (2016) Understanding the performance of optofluidic fuel cells: Experimental and theoretical analyses. Chem Eng J 283:1455-1464

Table list

Table 1 Comparison of the cell performance with existing works

Type of reactor	Anode Catalyst	Fuel	Electrolyte	Light source	V_{oc} (V)	I_{sc} (mA/cm^2)	P_{max} (mW/cm^2)	Refs.
Batch type	Pure TiO_2	Ethanol	0.1 mol/L TBAP	505 mW/cm^2 visible light	0.49	0.52	0.064	[38]
Batch type	10.0 % BiOI–TiO_2	20 mg/L BPA	0.05 mol/L Na_2SO_4	22 mW/cm^2 visible light	0.66	0.027	0.005	[39]
Batch type	Pure TiO_2	Methanol	0.1 mol/L TBAP	505 mW/cm^2 visible light	0.54	0.80	0.099	[40]
Batch type	Pure TiO_2	20 vol % Ethanol	0.2 mol/L NaOH	1.1 mW/cm^2 UV light	1.25	0.20	0.175	[41]
Micro type	TiO_2 nano-rod array	10 mg/L□ Methylene blue	1.25 mol/L NaOH	4.67 mW/cm^2 UV light	0.90	1.25	0.450	[42]
Micro type	Pure TiO_2	1 mol/L Methanol	0.5 mol/L KOH	6 mW/cm^2 UV light	1.16	0.65	0.400	This Work

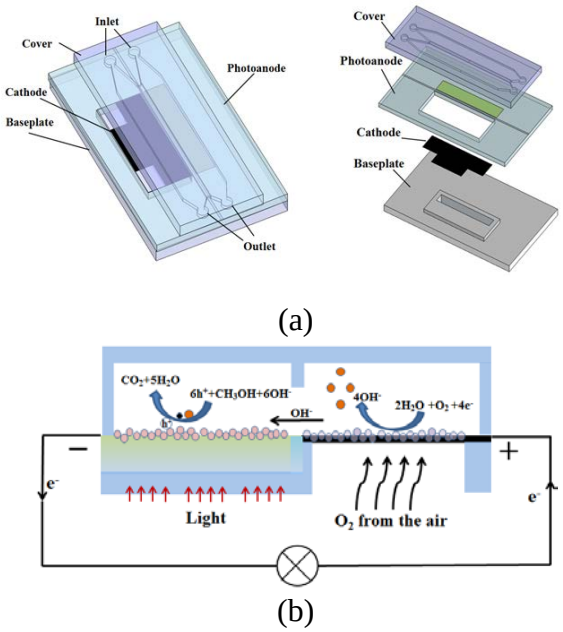

Fig. 1 (Color online) **a** Design of the membraneless and monolithic μPFC with the air-breathing cathode; **b** Working principle of the developed μPFC

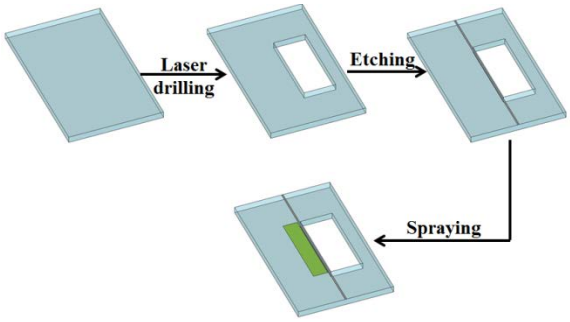

Fig. 2 (Color online)Illustration of the photoanode fabrication procedure

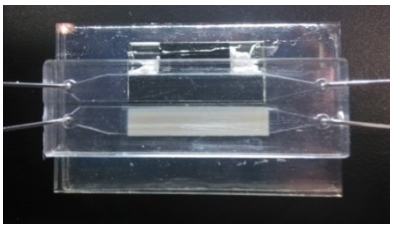

Fig. 3 (Color online) Image of the fabricated μPFC

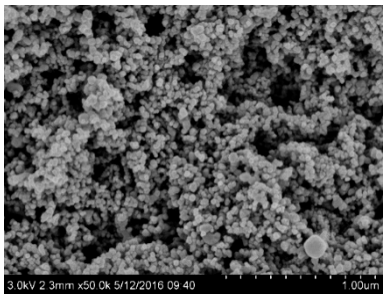

(a)

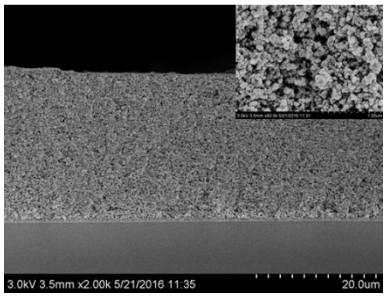

Fig. 4 The SEM images of TiO_2 film: (**a**) Top view and (**b**) cross sectional view

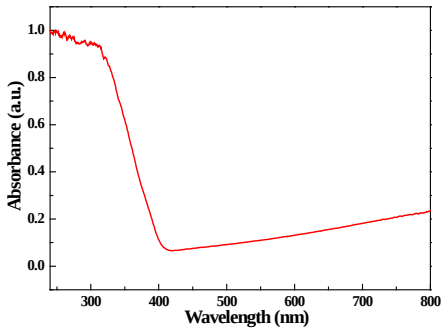

Fig. 5 (Color online) UV-Vis absorption spectra of the TiO_2 film

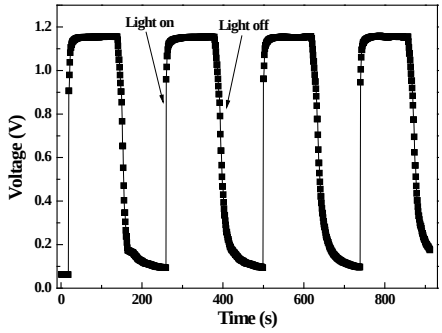

(a)

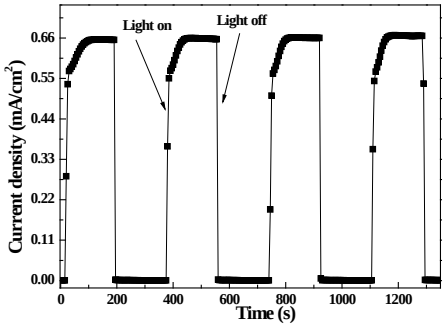

(b)

Fig. 6 a Photo-voltage response of the μPFC. **b** Photo-current response of the μPFC. Light intensity: 6 mW/cm^2; Methanol concentration: 1.0 mol/L; KOH concentration: 0.5 mol/L; Flow rate: 200 μL/min

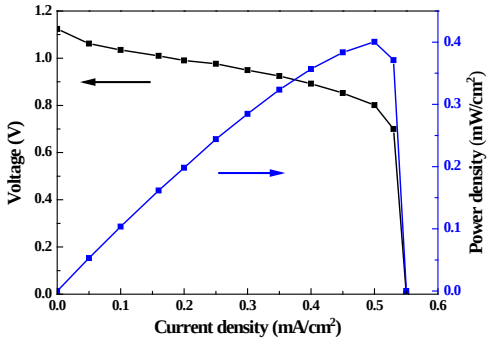

(a)

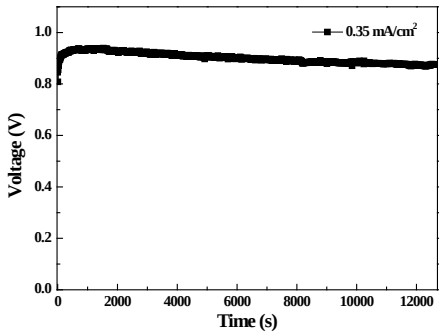

(b)

Fig. 7 (Color online) (**a**) Overall discharging performance of the μPFC. (**b**) Long-term discharging perormance of the μPFC. Light intensity: 6 mW/cm^2; Methanol concentration: 1.0 mol/L; KOH concentration: 0.5 mol/L; Flow rate: 200 μL/min

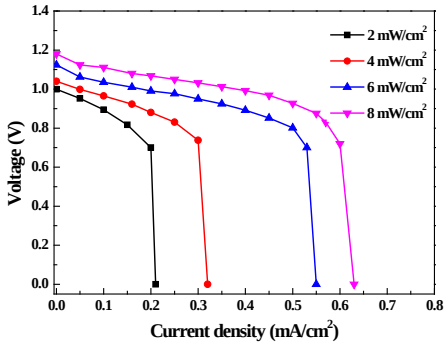

(a)

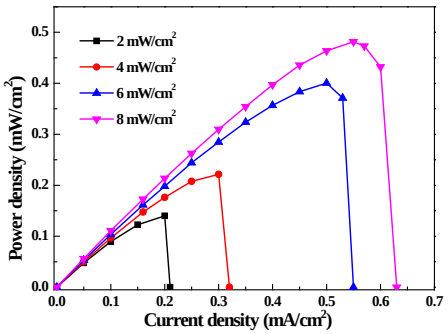

(b)

Fig. 8 (Color online) **a** Polarization curves of the μPFC at various light intensities. **b** Power density curves of the μPFC at various light intensities. Methanol concentration: 1.0 mol/L, KOH concentration: 0.5 mol/L; Flow rate: 200 μL/min

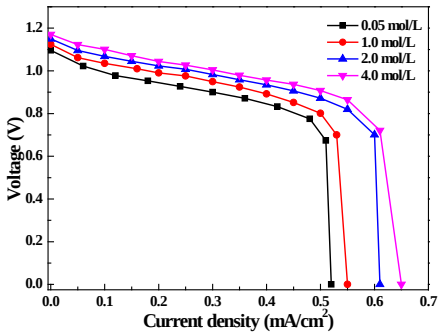

(a)

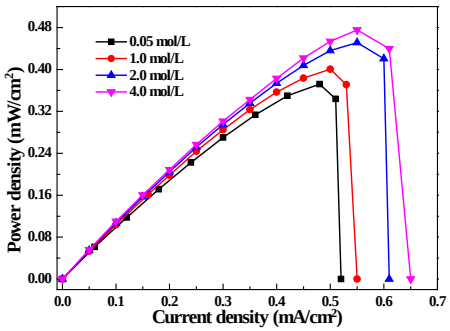

(b)

Fig. 9 (Color online) **a** Polarization curves of the μPFC at various methanol concentrations. **b** Power density curves of the μPFC at various methanol concentrations. Light intensity: 6 mW/cm^2; KOH concentration: 0.5 mol/L; Flow rate: 200 μL/min

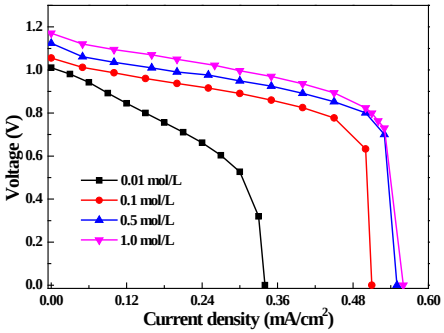

(a)

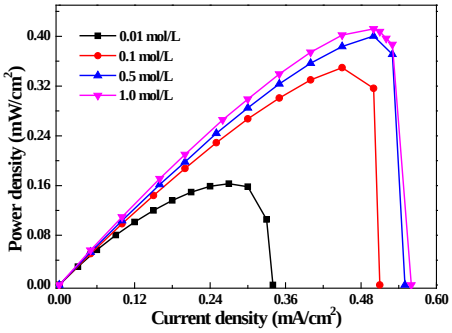

(b)

Fig. 10 (Color online) **a** Polarization curves of the μPFC at various KOH concentrations. **b** Power density curves of the μPFC at various KOH concentrations. Light intensity: 6 mW/cm^2; Methanol concentration: 1.0 mol/L; Flow rate: 200 μL/min

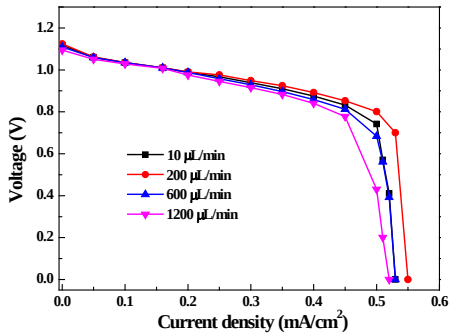

(a)

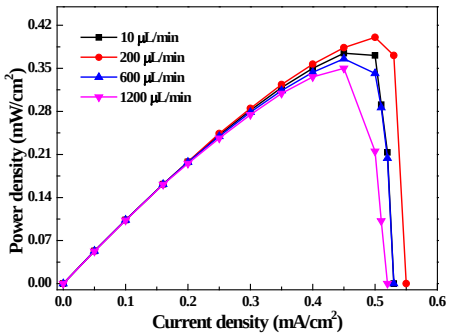

(b)

Fig. 11 (Color online) **a** Polarization curves of the μPFC at various flow rates. **b** Power density curves of the μPFC at various flow rates. Light intensity: 6 mW/cm^2; Methanol concentration: 1.0 mol/L; KOH concentration: 0.5 mol/L